Beilstein-Institut

Functional Nanoscience
May 17th – 21st, 2010, Bozen, Italy

Catalytic Nanomotor Function and Locomotion Physics

Jonathan D. Posner[1,*], Jeffrey L. Moran[1], Joseph Wang[2] and Philip Wheat[1]

[1]Mechanical & Aerospace Engineering, Chemical Engineering, Arizona State University, Tempe, AZ 85287, U.S.A.

[2]Department of Nanoengineering, University of California San Diego, La Jolla, CA 92093, U.S.A.

E-Mail: *jposner@asu.edu

Received: 20th August 2010 / Published: 13th June 2011

Introduction

In nature, microorganisms propel themselves through fluid media by mechanical deformation of solid appendages using energy they harvest from their local environment [4, 24, 36, 40]. Alternatively, Mitchell proposed that an asymmetric ion flux on a bacterium's surface could generate electric fields that drive locomotion via self-electrophoresis [27, 28, 41]. This proposed mechanism grew out of research on endogenous bioelectric fields which provided motive force in morphogenesis [13, 17, 25, 31]. Lund and Jaffe realized that asymmetric currents on the surface of a cell or embryo could generate bioelectric fields that alter the shape of cells and tissues as well as drive the transport of biomolecules. Roughly thirty years after Mitchell's hypothesis, Waterbury *et al.* [39] discovered that cyanobacteria are able to swim at speeds up to 25 μm s^{-1} without flagella, suggesting that they move by a non-mechanical propulsion mechanism. This theory was explored by Anderson (and later Lammert *et al.* [22]) who hypothesized that Waterbury's flagella-less cyanobacteria may swim due to Mitchell's self-electrophoretic mechanism [1]. Mitchell's self-electrophoresis mechanism and the subsequent analysis by Anderson were rejected for cyanobacteria by Pitta and Berg [35].

Recent advances in nanofabrication have enabled the engineering of synthetic analogues to those proposed by Mitchell that swim due to asymmetric ion flux mechanisms. Several realizations of synthetic swimmers, or artificial nanomotors, have been demonstrated. A common theme among these artificial swimmers is the production of species concentration gradients by asymmetric chemical or electrochemical reactions occurring on the surface of Janus particles [8, 11, 12, 16]. Electrochemical reactions have also been shown to drive the motion of colloidal particles. The particles effectively act as short-circuited electrochemical cells. Mano and Heller [26] demonstrated the propulsion of a carbon fibre by redox reactions of glucose and oxygen occurring on opposite sides of the fibre. Propulsion due to electrochemical reactions has also been demonstrated with decomposition of hydrogen peroxide. The peroxide undergoes two electrochemical half-reactions before finally yielding oxygen and water. Electrochemical peroxide decomposition has been reported to generate fluid flows above concentric electrodes [19] and in between interdigitated microelectrodes [34] as well as to propel rotating micro-gears made from platinum and gold [7] and bimetallic nanorod motors [23, 33, 38].

Bimetallic nanorods are high aspect ratio metallic cylinders, typically 2 μm in length and ≈300 nm in diameter. Swimming bimetallic rods were introduced to the community by Paxton *et al.* [32]. Laocharoensuk *et al.* [23] added hydrazine to the hydrogen peroxide solutions and incorporated carbon nanotubes into the platinum segments of Pt/Au rods to obtain nanomotor velocities in excess of 200 μm s^{-1} (100 body lengths per second). Kagan *et al.* [18] demonstrated that the nanomotors' velocity strongly depends upon the presence of ions in the solution. They showed that for most electrolytes, nanomotor speed decreases with increasing salt concentration; however, silver ions caused a fivefold increase in the nanomotors' speed. A nanomotor's velocity can be externally modulated by heat pulses [2] and by electrochemically controlling the local concentration of hydrogen peroxide and dissolved molecular oxygen [6].

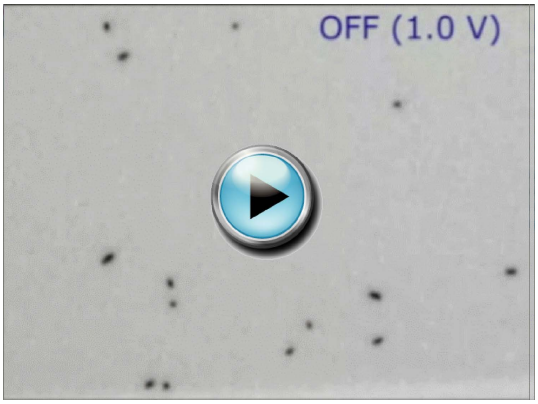

Movie 1. Electrochemical Switching of Nanomotors Motion.

Directional control of the nanomotors' motion has been achieved using external magnetic fields by incorporating a ferromagnetic segment, such as nickel, between the platinum and gold segments [5, 19]. We and others have shown that nanomotors can pick up, haul, and release micron-scale cargo [5, 37]. By hauling cargo of various sizes, we calculated that these nanomotors produce roughly 0.1 pN of force. In the case of bimetallic nanomotors, the mechanism by which asymmetric reactions generate forces and locomotion is not well understood. Several theories have been proposed. In their initial paper introducing the nanomotors [32], Paxton and co-workers proposed a propulsion mechanism based on the formation of gradients in interfacial tension. According to this mechanism, oxygen produced at the platinum end causes a local decrease in the interfacial tension between the aqueous solution and the gas-coated rod. The interfacial tension gradient then drives a Marangoni flow that results in a net propulsive force that drives particle motion. Although this theory predicts a propulsive force of the appropriate magnitude, it makes no predictions regarding the direction of particle motion. Paxton *et al.* [33] considered the possibility of motion due to a concentration gradient in molecular oxygen drives the particle due to diffusiophoresis. They found that the predicted diffusiophoretic velocity was much smaller than that observed in experiments and in the wrong direction. A later study showed that fluid could be pumped as a result of flows induced by electrochemical reactions occurring on concentric metallic electrodes [20]. This system was later studied analytically and experimentally using the Poisson, advection-diffusion, and Helmholtz-Smoluchowski equations [21].

The physics of this mechanism is similar to the self-electrophoretic mechanism proposed by Mitchell [27]. Although there is a growing consensus that Mitchell's self-electrophoretic mechanism is important in the motion of bimetallic nanomotors, many key physical details of the remain unexplained.

Here we are interested in locomotion of particles that are driven due to concentration and potential gradients that are generated by reactions occurring on the particle surface. We present some experimental results describing the controlled motion of catalytic nanomotors as well as some numerical simulations on the physical mechanisms underlying the locomotion of particles due to asymmetric reactions. Since we solve the full equations for conservation of mass, species, and momentum as well as Poisson's equation for electric potential, our model incorporates all effects due to diffusiophoresis, chemiphoresis, and electrophoresis. The simulations provide quantitative predictions of the nanomotor's swimming velocity for a given surface charge and reaction rate. We observe excellent agreement between experiments with our scaling analysis and numerical models.

Description of the Problem

Figure 1 shows a schematic of a platinum-gold nanorod in an aqueous hydrogen peroxide solution. If the rod is immersed in a hydrogen peroxide solution, catalytic electrochemical reactions occur on its surface. On the platinum end, an oxidation reaction decomposes

peroxide into protons, electrons, and oxygen molecules. The oxidation reaction results in a local depletion of the peroxide fuel and abundance of protons and oxygen. The electrons conduct through the rod from platinum to gold. At the gold end, two reduction reactions are possible which both result in the production of water. First, protons, electrons, and peroxide react to form water. Second, molecular oxygen, protons, and electrons can react to generate water. At the Au end there is a net depletion of protons and, to a lesser extent, peroxide and molecular oxygen. In this way, the nanomotor effectively functions as a short-circuited galvanic cell which generates a surface flux of protons at the anode (Pt end) and consumes protons at the cathode (Au end). This basic description of the reaction mechanism was used by Wang *et al.* [38] to successfully predict the direction of motion of a nanomotor composed of any two of six noble metals.

Here we provide a model that shows that the locomotion is driven by fluid slip around the nanomotor caused by self-generated electrical body forces in a mechanism called reaction induced charge auto-electrophoresis (RICA) [29, 30]. The respective excess and depletion of protons at the anode and cathode generate an electric field, $\boldsymbol{E}$. Electric body forces, of the form $\rho_e \boldsymbol{E}$, arise due to the coupling of free charge density, ρ_e, with tangential electric fields which are generated by the asymmetric charge density distribution induced by the asymmetric surface reactions. The charge density results from the asymmetry in cation concentration (due to the reactions, as shown in Figure 1) as well as from the diffuse portion of the electric double layer (EDL) that forms due to the rod's native surface charge (not shown in Figure 1). The electric body forces drive fluid motion and thus nanomotor motion. Ultimately, net locomotion is driven by a coupling of the diffuse charge in the EDL that shields native surface charge on nanomotor surface and electric fields that are driven by the asymmetric distribution of reaction products established by the heterogeneous surface reactions.

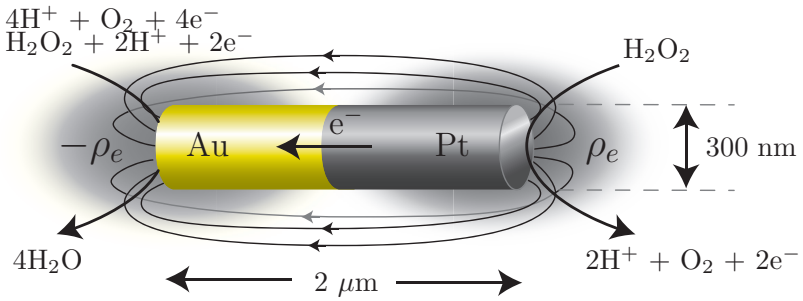

Figure 1. Schematic of Pt/Au catalytic nanomotor in hydrogen peroxide solution showing typical dimensions, electrochemical reactions, approximate charge density distribution, and approximate electric field lines. As shown here, the rod's motion is directed to the right.

EXPERIMENTS

Experimental Methodology

The magnetic nanomotors were prepared by electrodepositing the corresponding metals or hybrid metal-CNT composite into a porous alumina membrane template (Catalogue no. 6809 – 6022; Whatman, Maidstone, U.K.). A thin gold film was first sputtered on the branched side of the membrane to serve as a working electrode. The membrane was assembled in a plating cell with aluminium foil serving as an electrical contact for the subsequent electro-deposition. In order to synthesize well-shaped cylindrical nanomotors, a sacrificial silver layer was electrodeposited into the branched area (1 – 2 μm thickness) of the membrane using a silver plating solution (1025 RTU@4.5 Troy/Gallon; Technic Inc., Anaheim, CA, U.S.A.) and a total charge of 2 coulombs (C) at -0.9 V (vs. Ag/AgCl, in connection to a Pt wire counter electrode). This was followed by the electro-deposition of gold (0.75 C) from a gold plating solution (Orotemp 24 RTU RACK; Technic Inc.) at -0.9 V (vs. Ag/AgCl). Following the plating of the first gold segment (0.75 C), nickel was electrodeposited from a nickel plating solution 20 g l^{-1} $NiCl_2 \cdot 6\,H_2O$, 515 g l^{-1} $Ni(H_2NSO_3)_2 \cdot 4\,H_2O$, and 20 g l^{-1} H_3BO_3 (buffered to pH 3.4)] at -1.0 V (vs. Ag/AgCl). A total charge of 2.0 C was used for plating nickel. The second gold segment (0.75 C) was then deposited. Subsequently, platinum-CNT were deposited galvanostatically at -2 mA for 50 min from a platinum plating solution containing 0.50 mg/ml of CNT, along with 0.1 wt% Nafion and 2 mM 4-nitrobenzenediazonium tetrafluoroborate, respectively. After depositing the nanomotors, the membrane was removed from the plating cell and rinsed thoroughly with nanopure water to remove all residues. The sputtered gold layer and the silver layer were simultaneously removed by mechanical polishing using cotton tip applicators soaked with 35% HNO_3 for ca. 5 min to ensure complete silver dissolution. The nanomotors were then released by immersing the membrane in 3 M NaOH for 30 min. These nanowires were collected by centrifugation at 10,000 rpm for 5 min and washed repeatedly with nanopure water (18.2 M cm) until a neutral pH was achieved. Between washing steps the nanowire solution was mixed and briefly sonicated (several seconds) to ensure the complete dispersion of nanowires in the washing water and hence the removal of salt residuals entrapped in the nanowire aggregate after centrifugation.

Special attention was paid to the nanowires being washed directly before testing and suspended in freshly obtained nanopure water due to significant deceleration of the nanomotors speed in the presence of salt ions. All nanomotors were stored in nanopure water at room temperature and their speed tested within a day of synthesis.

The nanomotor suspensions were diluted in water and mixed with hydrogen peroxide solution to obtain roughly 5 wt% H_2O_2, unless noted. The real-time movement of the nanomotors was visualized using white light transmission microscopy at 200 × total magnification (Nikon Instrument Inc., Eclipse80i, Melville, NY, U.S.A.) equipped with a Photo-

metrics CoolSnap CF camera (Roper Scientific, Duluth, GA, U.S.A.). The nanomotors where controlled using a 9.5 mm cube-shaped Neodymium (NdFeB) magnet placed at the centre of the top face of a larger 25.4 mm NdFeB cube shaped magnet (both 1.32 Tesla from K&J Magnetics Inc., Jamison, PA, U.S.A.). The magnet pair was fixed to a custom magnet holder, and attached directly to the microscope condenser stage thus aligning the centre of the magnets with the optical axis.

The magnetic poles (from north to south) of the large and small magnets were opposite in direction while both were perpendicular to the optical axis of the microscope. The superposition of the magnetic fields of the two magnets allowed for a weak parallel magnetic field at a distance greater than 2 mm and a strong perpendicular field ca. 1 mm. For cargo pickup and release experiments a diluted suspension of nanomotors and magnetic-nanoparticles coated polystyrene beads (Spherotech, Inc., Libertyville, IL, U.S.A.) was prepared. A 10 mm cube-shaped magnet was placed on the microscope stage next to a microcapillary tube, containing the nanomotors and spherical cargo. To measure the speeds of a nanomotor before picking up, during transporting and after dropping off the cargo, the nanomotor was magnetically directed toward an unbound magnetic microsphere, captured and transported it for ca. 5 seconds and finally releasing the cargo via a fast reversal of the magnetic poles.

Results

We demonstrate the directed motion of catalytic nanomotors and their cargo transport and manipulation capabilities along predetermined paths within micro-channel networks. We eliminate the requirement for functionalization of the nanowire by making use of the magnetic properties of a nickel segment for guiding and sorting of nanomotors through various junctions of the microfluidic network at speeds up to 40 μm s^{-1}. In addition, the magnetic segments enable dynamic loading, transport, and release of spherical magnetic cargo. The ability of a nanomotor to travel on a predetermined path is an important aspect of the integration of nanomotors into microfluidic networks. Directed motion of chemically-powered Au/Ni/Au/Pt-CNT nanowires within a micro-channel network is illustrated in Figure 2. A weak external magnet was used for sorting the nanomotors in each of the junctions of the microfluidic network, without contributing to the nanomotors speed. For example, Figure 2A illustrates a 2 μm long Au/Ni/Au/Pt-CNT nanomotor travelling in an hourglass pattern along a 700 μm long preselected path in a symmetric central portion of the micro-channel network over a 70 second period. Figure 2B illustrates the directional manipulation of the nanomotors within the micro-channel network. Four predetermined paths (a-d), starting from the same starting point (SP), illustrate the dexterity of the CNT-based nanomotors and the magnetic sorting in different junctions. It should be noted that the same nanowire was travelling continuously in all four paths of Figure 2B (as well as returning to the same starting point) for more than an hour.

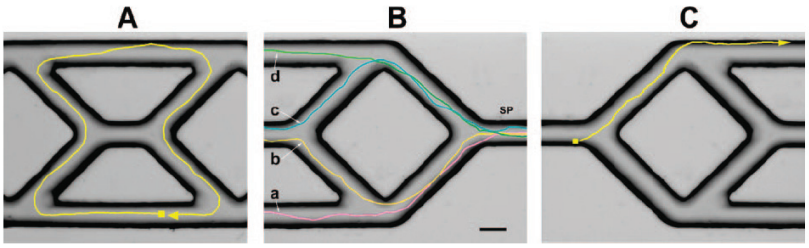

Figure 2. Tracks of directed nanomotor movement within a microfabricated channel network. **(A)** Motion of an Au/Ni/Au/Pt-CNT nanomotor maneuvering around the central portion of a PDMS microstructure. **(B)** Motion of the same nanowire over four different paths (a-d) beginning from the same starting point (SP). **(C)** Motion of a nanomotor in a mixed peroxide/hydrazine fuel. Fuels, 5 wt% H_2O_2 **(A, B)**; 2.5 wt% H_2O_2/0.15 wt% hydrazine **(C)**. Scale bar 25 μm. Reprinted with permission from [5]. Copyright 2010 American Chemical Society.

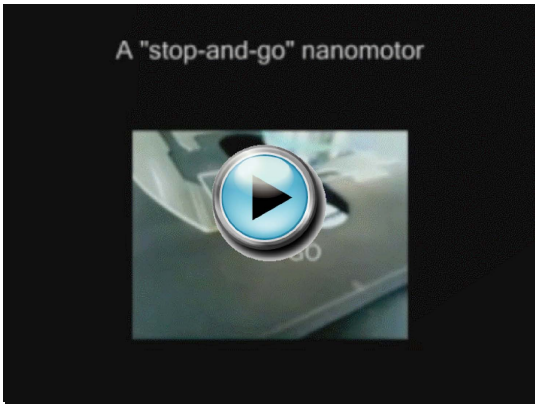

Movie 2. A "stop-and-go" nanomotor.

The magnetic properties of the Au/Ni/Au/Pt-CNT nanomotor can also be exploited for executing a controlled pick up and release of the magnetic-spherical cargo as shown in Figure 3 [5]. On-demand cargo pick up is accomplished by a weak magnetic interaction between the superparamagnetic spherical particle and the ferromagnetic nickel segment in the nanomotor. The nanomotor is directed close to the spherical particle. When the nanomotor is in close proximity to the particle, (ca. one particle diameter) the magnetic fields of the particle and nanomotor are sufficient to bring them together. The spherical particle-nanomotor complex continues to move, powered by RICA, along the path dictated by the external magnetic field. Release is accomplished by exploiting the weak interaction between the nickel segment within the nanomotor and the magnetic polystyrene beads. A fast change in the direction of the nanomotor (through rapid 180 degree rotation of the external magnet)

releases the magnetic cargo when the viscous fluid drag on the particle exceeds the magnetic force between the nanowire and the particle. This cargo manipulation functionality could be used for controlled assembly, autonomous microdevices, or drug delivery, for example.

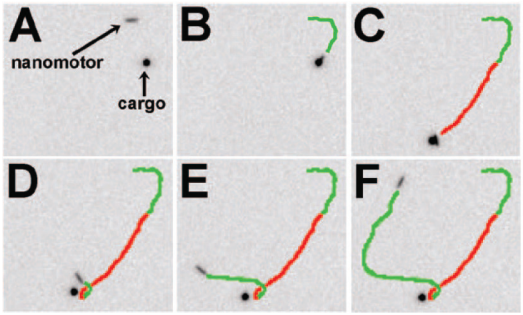

Figure 3. Sequential micrographs **(A-F)** of cargo pickup, transport, and release by an Au/Ni/Au/Pt-CNT nanomotor. Green and red traces denote the path traveled by the nanomotor and the cargo-loaded nanomotor, respectively: (**A** and **B**) the manipulation toward and pickup of cargo by a nanomotor; **(C)** subsequent transport of the cargo by the nanomotor; **(D)** release of the cargo; (**E** and **F**) motion of the nanomotor after the cargo release. Reprinted with permission from [5]. Copyright 2008 American Chemical Society.

Movie 3. In-dive cargo pick-up by magnetic controlled synthetic nanomotors.

We measure the velocity of the nanomotor-particle complexes and find that that they depend on the size of the cargo. Figure 4 shows the velocity of the complex as a function of the size of the particle diameter. This plot shows that the nanomotor velocity decreases from 11 to 4 µm s^{-1} upon increasing the cargo size from 1.3 to 4.3 µm, respectively.

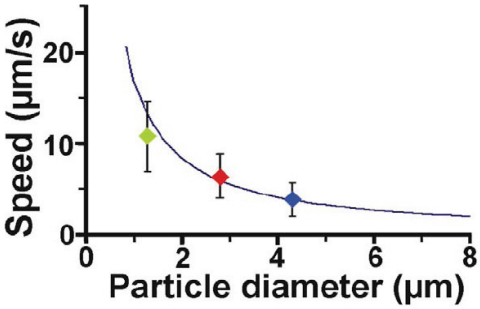

Figure 4. Nanomotor-sphere complex velocity as a function of the attached sphere diameter. The solid line is a simple theory based on the Stokes drag of the sphere. Reprinted with permission from [5]. Copyright 2010 American Chemical Society.

We expect that the complexes' velocity to depend on the size of particle because the speed of the terminal velocity of the nanomotor is reached when the propulsive force of the electrokinetic locomotion is balanced with the hydrodynamic Stokes drag as,

$$F_d = F_{nm} = 6\pi\mu Ua,$$

where μ is the fluid viscosity, U the velocity of the nanomotor complex, a is the particle radius, F_d is the drag force, and F_{nm} is the force the nanomotor generates due to RICA. Using this equation, we can make a theoretical prediction of the complexes' velocity as a function of the cargo diameter. This prediction is shown along with the experimental data in Figure 4. This theory requires a single fitting parameter, namely the force generated by the nanomotor. We find that fitting this theory to the data results in a nanomotor force of 0.16 pN. Smaller forces (0.04 pN) have been reported for conventional (undoped) Pt-Au nanowires. The larger cargo-towing forces of the CNT-based nanomotors allow transport of larger cargo at a faster speed compared to common Pt-Au nanowires (e. g., 4 μm/s for the 4.3 μm cargo compared to 3.5 μm/s for the 2.1 μm cargo, respectively).

We have also measured the velocity of nanomotors as a function of peroxide concentration. Figure 5 shows the velocity of undoped nanomotors as a function of peroxide wt%. We obtained the experimental data in Figure 5 by measuring the velocity of approximately 200 nanomotors using optical microscopy in varying concentrations of hydrogen peroxide. The value of j/j_d at each peroxide concentration is estimated from the published dependence of electrocatalytically generated current density on Pt and Au interdigitated microelectrodes [34]. We have subtracted out the characteristic Brownian velocity of the nanomotors (measured here to be 4.87 μm s^{-1}) from all experimental data points in order to only consider the axial velocities measured in the experiments. The velocity increases linearly with peroxide concentration. We also make predictions of this velocity as a function of the current density and zeta potential of the rod as will be discussed in the following section.

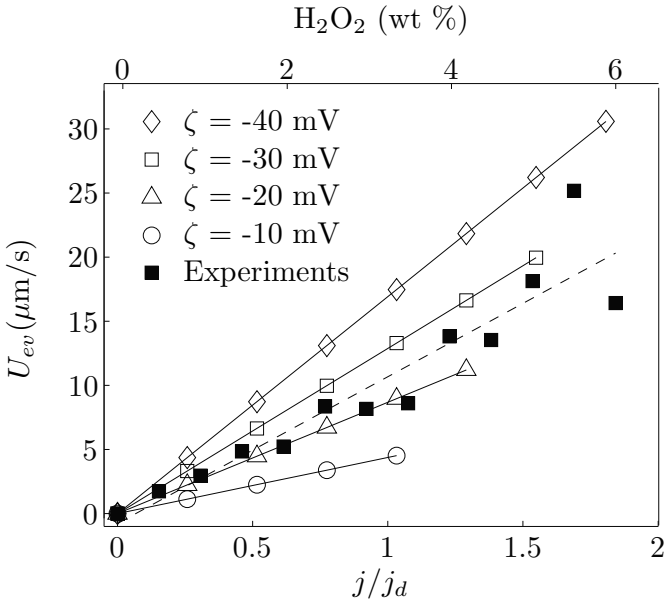

Figure 5. Nanomotor velocity as a function of dimensionless flux j/j_d (lower axis) and hydrogen peroxide concentration (upper axis). Simulations (open symbols), the scaling analysis (lines), and experiments (closed symbols) show excellent agreement. Simulations are shown for four values of the zeta potential. Copyright (2008) by the American Physical Society.

Movie 4. Nanomotors in 1% Hydrogen Peroxide

Movie 5. Nanomotors in 3% Hydrogen Peroxide. The movies show that the velocity of the motors increases with peroxide concentration.

Theory and Simulations

Here we present detailed simulations, scaling analysis, and experiments that describe the locomotion of bimetallic nanomotors in hydrogen peroxide solutions due to Reaction Induced Charge Auto-Electrophoresis (RICA) [29, 30]. Nanomotor movement is the result of an electroviscous slip velocity that is driven by electrical body forces resulting from charge density and electric fields that are internally generated by electrochemical reactions occurring on the particle surface. We expect that a detailed understanding of the physics underlying the nanomotors' motion will provide a basis for rational design of next-generation nanomachines capable of operation in diverse conditions and applications.

In our model, we consider a rod immersed in a binary electrolyte with equal concentrations of H^+ and OH^- ions. In the dilute solution limit, the steady ion concentration distributions are given by the advection-diffusion equation,

$$u \cdot \nabla c_i = D_i \nabla^2 c_i + z_i F \nu_i \nabla \cdot (c_i \nabla \phi), \tag{1}$$

where u is the fluid velocity, c is the molar concentration, D is the diffusivity, z is the valence, F is the Faraday constant, ν is the mobility, ϕ is the electrostatic potential, and the subscript i denotes the species. The electrostatic potential in turn depends on the local free charge density as described by the Poisson equation,

$$-\epsilon \nabla^2 \phi = \rho_e = F(z_+ c_+ + z_- c_-), \tag{2}$$

where $z_+ = 1$, $z_- = -1$, ρ_e is the volumetric charge density, and $\varepsilon = \varepsilon_r \varepsilon_0$ is the permittivity of the liquid which we assume to be constant. In our model, fluid motion (and thus nanomotor motion) is driven by electrical body forces, which depend on the concentrations of charged species only. We and others have estimated the forces due to diffusiophoresis and found that they are several orders of magnitude smaller than those produced by the induced charge mechanism described here [33]. For this reason we do not consider the oxygen and peroxide concentrations and focus on a simple binary electrolyte. To close the system of equations we include the steady, incompressible Navier-Stokes equations for a Newtonian fluid,

$$\nabla \cdot u = 0 \tag{3}$$

$$\rho(u \cdot \nabla u) = -\nabla p + \eta \nabla^2 u - \rho_e \nabla \phi. \tag{4}$$

Here ρ is the fluid density, p is the pressure, η is the dynamic viscosity, and $\rho_e \nabla \phi$ is the electrical body force that results from the coupling of charge density and electric field. This general framework has been used extensively to describe electrohydrodynamic flows [15], particularly electrokinetic flows which are driven by a coupling of externally applied fields and charged objects.

The reactions are represented by boundary conditions specifying the molar proton fluxes on the surface of the nanomotor. On the anode and cathode we prescribe equal and opposite fluxes *j* and *-j* normal to the wire surface. Since anions (hydroxide ions) do not participate in the reactions, the normal anion flux is set to zero everywhere on the nanomotor surface. The values of the proton fluxes specified in the simulations are based on previously published measurements of current density at Pt and Au electrodes in hydrogen peroxide [6, 23, 34]. Here we do not directly model the electrochemical reactions that are described by the Butler-Volmer equation, because we have direct measurements of the current density for our electrocatalysts and fuel. At the nanomotor surface we apply the no-slip condition for the velocity and specify the local surface potential (relative to the bulk solution) as $\phi = \xi$. Far from the rod surface, the electrostatic potential decays to zero and ion concentrations approach their bulk value, i.e., $\phi \to 0$ and $c_i \to c_\infty$ as the radial distance $r \to \infty$.

We non-dimensionalize the momentum equation using the following scaling quantities: $|u| \propto U_{ev}$, $p \propto \eta U_{ev}/d$, $\rho_e \propto \rho_{e_0}$, and $\nabla\phi \propto E_0$ where ρ_{e_0} is a characteristic charge density, E_0 is a characteristic electric field, d is a viscous length scale, and U_{ev} is a characteristic electroviscous velocity. Applying these scalings to the momentum equation (4), a Reynolds number emerges based on the electroviscous velocity, given by $Re = \rho U_{ev} d/\eta$. Here we use the electroviscous velocity which arises in electrokinetic systems due to the balance of electrical body and viscous forces acting on the fluid, defined as [15]

$$U_{ev} \equiv \frac{\rho_{e_0} E_0}{\eta / d^2}. \tag{5}$$

Metallic nanorods support a native surface charge in aqueous solutions [9]. The charged surface attracts a screening cloud of counter-ions which develops a region of net charge density in the electrical double layer (EDL) surrounding the rod. The characteristic length scale of the charge density region is the Debye thickness λ_D, which scales with the background electrolyte concentration ${c_\infty}^{-1/2}$. This charge density in the EDL scales with the potential in the EDL based on the Poisson-Boltzmann equation for a symmetric binary electrolyte,

$$\rho_{e_0} \propto \frac{2z^2F^2c_\infty\zeta}{RT} \propto \frac{\epsilon\zeta}{\lambda_D^2}, \tag{6}$$

where $z = 1$ and we have imposed the Debye-Hückel approximation. In order to also include the effects of the reaction-driven flux, we introduce a characteristic electric field based on the flux and diffusivity of protons,

$$E_0 \propto \frac{F\lambda_D h}{\epsilon D_+} j, \tag{7}$$

where h is the length of the nanomotor and also the characteristic length for the electric field. Combining expressions (5 – 7), the electroviscous velocity scales as

$$U_{ev} \propto \frac{\zeta F h \lambda_D}{\eta D_+} j. \tag{8}$$

Here we scale the viscous length scale d with the EDL thickness λ_D since the region of significant viscous and electrical body forces is limited to the area with charge density. As shown in Figure 6B, the z-component of the self-generated electric field is significant along a distance that scales with the nanomotor length h. The scaling analysis shows that the nanomotor speed increases linearly with the reaction flux j because the flux generates charge density which produces the internally generated field. Equation 8 can be recast in the form of the Helmholtz-Smoluchowski equation $U_{ev} = \epsilon\zeta E_0/\eta$ which describes the electrophoretic velocity for a charged particle in the presence of an external electric field [14], where here E_0 is given by equation 7.

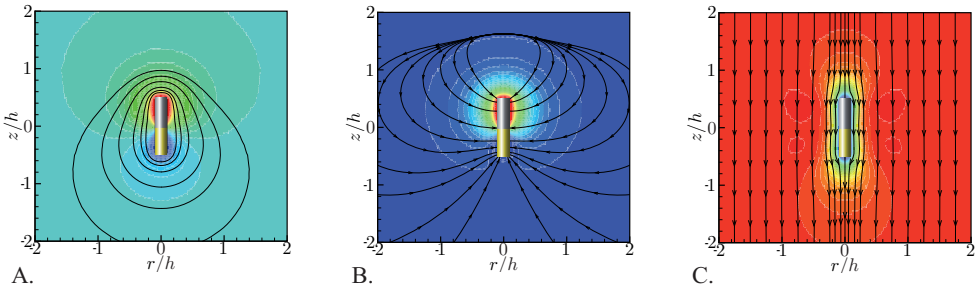

Figure 6. Simulation-generated plots of **(A)** normalized proton concentration c^* (color-red and blue denote high and low proton concentrations, respectively) and electrical potential Φ^* (contour lines), **(B)** charge density ρ_e (color- red denote positive charge density above background zero levels in blue) and electric field (streamlines) and **(C)** RICA velocity magnitude (colors – blue is zero and red is maximum velocity) and streamlines (black lines) for the case $\zeta = -10$ mV and $j/j_d = 0{:}8$. The reactions lead to an asymmetry in the proton concentration such that an excess of protons builds up at the anode and protons are depleted at the cathode. The excess of protons results in positive charge density at the anode and the generation of electric field pointing from the anode to the cathode. Copyright (2010) by the American Physical Society.

We assume the flow is axisymmetric and thus solve the system over a two-dimensional cross-section of the 3-D problem. The 100 μm × 100 μm simulation domain is discretized into approximately 181,000 triangular mesh elements. The length and diameter of the simulated nanomotor are set to 2 μm and 370 nm, respectively. We solve the system of governing equations (1 – 4) numerically using the linear system solver PARDISO. Using a two-ion model with a fixed bulk electrolyte concentration, the only free parameters in the system are the nanomotor native surface potential ζ and the surface flux *j*. We normalize the flux by characteristic flux based on Nernst's diffusion limited current density given by $j_d = 4D_+c_\infty/\lambda_D$ [3].

Figure 6A shows the dimensionless proton concentration $c^* = (c_+ - c_\infty)/c_\infty$ (colour) and contours of the electric potential normalized by the thermal voltage $\phi^* = zF\phi/RT$ (black lines) for the case where $\xi = -10$ mV and $j/j_d = 0.8$. In the absence of reactions, the EDL proton concentration and electrical potential are both symmetric around the nanorod. Figure 6A shows that when reaction-driven fluxes are introduced, an asymmetry in the proton concentration is established such that an excess of protons builds up at the anode and protons are depleted at the cathode. The reactions also result in an asymmetric electrical potential profile that bulges at the cathode.

Figure 6B shows the charge density and streamlines of electric field for the same case as Figure 6A. The charge density in the diffuse layer of the anode is positive because the negatively charged surface attracts cations near the surface and the surface reactions constantly inject cations. At the cathode the deficiency of protons due to reactions and the shielding protons due to the negatively charged surface nearly counteract each other result-

ing in weak negative charge density. The charge density generates an electric field, as described mathematically by Poisson's equation. The electric field couples with the charge density to produce an electrical body force, $\rho_e \boldsymbol{E}$, which acts on the fluid to drive an electroviscous velocity and propel the nanomotor.

Figure 6C shows the RICA velocity magnitude (colour) and streamlines (black lines). These simulations are conducted in the reference frame of the nanomotor. Fluid flows from the anode to the cathode due to electrical body forces that result from a coupling of positive charge density and electric field tangent to the nanomotor surface. By Galilean invariance, this is equivalent to the nanomotor swimming with the anode end forward.

Figure 5 shows the nanomotor velocity as a function of the flux j/j_d obtained from simulations, the scaling analysis, and experiments. The experiments and simulations show good agreement for a native surface potential of -25 mV, which we obtain from independent measurements of the zeta potential for Au and Pt particles in aqueous solutions [9, 10]. The simulations, scaling analysis, and experiments all show that the electroviscous swimming velocity of the nanomotors increase linearly with increasing peroxide concentration or current density.

Summary

Nobel Laureate Peter Mitchell originally proposed that an asymmetric ion flux across an organism's membrane could generate electric fields that drive locomotion. Although this locomotion mechanism was later rejected for some species of bacteria, modern nanofabrication tools have been harnessed to engineer bimetallic Janus particles that swim by ion fluxes generated by asymmetric electrochemical reactions. Here we have presented governing equations, scaling analyses, and numerical simulations that describe the motion of bimetallic rod-shaped motors in hydrogen peroxide solutions due to reaction-induced charge auto-electrophoresis. Our simulations show strong agreement with the scaling analysis and experiments. The analysis shows that electrokinetic locomotion results from electro-osmotic fluid slip around the nanomotor surface.

We have demonstrated the controlled motion of the nanomotors through micro-channel networks. We have shown that external magnetic field control of the motors can be used to pick-up, drag, and release micron scale colloidal cargo. Synthetic nanomachines may pave the way to integrated functional microdevices powered by autonomous transport.

Acknowledgements

The authors acknowledge Jared Burdick, Rawiwan Laocharoensuk, Kamil Salloum, Marcus Herrmann for contributions and stimulating discussions. This work was sponsored by NSF graduate fellowships to JLM and PMW and grants CBET-0853379 and CHE 0506529.

References

[1] Anderson, J.L. (1989) Colloid transport by interfacial forces. *Annu. Rev. Fluid Mech.* **21**:61 – 100.
doi: 10.1146/annurev.fl.21.010189.000425.

[2] Balasubramanian, S., Kagan, D., Manesh, K.M., Calvo-Marzal, P., Flechsig, G.-U., and Wang, J. (2009) Thermal modulation of nanomotor movement. *Small* **5**(13):1569 – 1574.
doi: 10.1002/smll.200900023.

[3] Bazant, M.Z., Chu, K.T., and Bayly, B.J. (2005) Current-voltage relations for electrochemical thin films. *SIAM J. Appl. Math.* **65**(5):1463 – 1484.
doi: 10.1137/040609938.

[4] Brennen, C. and Winet, H. (1977) Fluid mechanics of propulsion by cilia and flagella. *Annu. Rev. Fluid Mech* **9**(1):339 – 398.
doi: 10.1146/annurev.fl.09.010177.002011.

[5] Burdick, J., Laocharoensuk, R., Wheat, P.M., Posner, J.D. and Wang, J. (2008) Synthetic nanomotors in microchannel networks: Directional microchip motion and controlled manipulation of cargo. *J. Am. Chem. Soc.* **130**(26):8164 – 8165.
doi: 10.1021/ja803529u.

[6] Calvo-Marzal, P., Manian Manesh, K., Kagan, D., Balasubramanian, S., Cardona, M., Flechsig, G.-U., Posner, J. and Wang, J. (2009) Electrochemically-triggered motion of catalytic nanomotors. *Chem. Commun.* **30**:4509 – 4511.
doi: 10.1039/b909227g.

[7] Catchmark, J.M., Subramanian, S. and Sen, A. (2005) Directed rotational motion of microscale objects using interfacial tension gradients continually generated via catalytic reactions. *Small* **1**(2):202 – 206.
doi: 10.1002/smll.200400061.

[8] Córdova-Figueroa, U.M. and Brady, J.F. (2008) Osmotic propulsion: The osmotic motor. *Phys. Rev. Lett.* **100**(15).
doi: 10.1103/PhysRevLett.100.158303.

[9] Dougherty, G.M., Rose, K.A., Tok, J.B., Pannu, S.S., Chuang, F.Y.S., Sha, M.Y., Chakarova, G. and Penn, S.G. (2008) The zeta potential of surface-functionalized metallic nanorod particles in aqueous solution. *Electrophoresis* **29**(5):1131 – 1139.
doi: 10.1002/elps.200700448.

[10] Du, H.-Y., Wang, C.-H., Hsu, H.-C., Chang, S.-T., Chen, U.-S., Yen, S.C., Chen, L.C., Shih, H.-C., and Chen, K.H. (2008) Controlled platinum nanoparticles uniformly dispersed on nitrogen-doped carbon nanotubes for methanol oxidation. *Diamond and Related Materials* **17**(4 – 5):535 – 541.
doi: 10.1016/j.diamond.2008.01.116.

[11] Gibbs, J.G. and Zhao, Y.P. (2009) Autonomously motile catalytic nanomotors by bubble propulsion. *Appl. Phys. Lett.* **94**(16).
doi: 10.1063/1.3122346.

[12] Golestanian, R., Liverpool, T.B. and Ajdari, A. (2005) Propulsion of a molecular machine by asymmetric distribution of reaction products. *Phys. Rev. Lett.* **94**(22).
doi: 10.1103/PhysRevLett.94.220801.

[13] Harold, F.M., Bronner, F., Slayman, C.L., and Kleinzeller, A. (1982) Pumps and currents: A biological perspective. *In* Electrogenic Ion Pumps, volume 16 of *Current Topics in Membranes and Transport*, pages 485 – 516. Academic Press.

[14] Henry, D.C. (1931) The cataphoresis of suspended particles. part i. the equation of cataphoresis. *Proceedings of the Royal Society of London*. Series A, Containing Papers of a Mathematical and Physical Character 133(821):106 – 129.
doi: 10.1098/rspa.1931.0133.

[15] Hoburg, J.F. and Melcher, J.R. (1976) Internal electrohydrodynamic instability and mixing of fluids with orthogonal field and conductivity gradients. *J. Fluid Mech.* **73**(2):333 – 351.
doi: 10.1017/S0022112076001390.

[16] Ismagilov, R.F., Schwartz, A., Bowden, N. and Whitesides, G.M. (2002) Autonomous movement and self-assembly. *Angew. Chem., Int. Ed.* **41**(4):652 – 654.
doi: 10.1002/1521-3773(20020215)41:4<652::AID-ANIE652>3.0.CO;2-U.

[17] Jaffe, L.F. and Nuccitelli, R. (1974) Ultrasensitive vibrating probe for measuring steady extracellular currents. *J. Cell Biol.* **63**(2):614 – 628.
doi: 10.1083/jcb.63.2.614.

[18] Kagan, D., Calvo-Marzal, P., Balasubramanian, S., Sattayasamitsathit, S., Manesh, K.M., Flechsig, G.-U. and Wang, J. (2009) Chemical sensing based on catalytic nanomotors: Motion-Based detection of trace silver. *J. Am. Chem. Soc.* **131**(34):12082.
doi: 10.1021/ja905142q.

[19] Kline, T.R., Paxton, W.F., Mallouk, T.E. and Sen, A. (2005) Catalytic nanomotors: Remote-controlled autonomous movement of striped metallic nanorods. *Angew. Chem., Int. Ed.* **44**(5):744 – 746.
doi: 10.1002/anie.200461890.

[20] Kline, T.R., Paxton, W.F., Wang, Y., Velegol, D., Mallouk, T.E. and Sen, A. (2005) Catalytic micropumps: Microscopic convective fluid flow and pattern formation. *J. Am. Chem. Soc.* **127**(49):17150 – 17151.
doi: 10.1021/ja056069u.

[21] Kline, T.R., Iwata, J., Lammert, P.E., Mallouk, T.E:, Sen, A. and Velegol, D. (2006) Catalytically driven colloidal patterning and transport. *J. Phys. Chem. B* **110**(48):24513 – 24521.
doi: 10.1021/jp064393l.

[22] Lammert, P.E., Prost, J. and Bruinsma, R. (1996) Ion drive for vesicles and cells. *J. Theor. Biol.* **178**(4):387 – 391.
doi: 10.1006/jtbi.1996.0035.

[23] Laocharoensuk, R., Burdick, J. and Wang, J. (2008) Carbon-nanotube-induced acceleration of catalytic nanomotors. *ACS Nano* **2**(5):1069 – 1075.
doi: 10.1021/nn800154g.

[24] Lauga, E. and Powers, T.R. (2009) The hydrodynamics of swimming microorganisms. *Rep. Prog. Phys.* **72**(9).
doi: 10.1088/0034-4885/72/9/096601.

[25] Lund, E.J. (1947) Bioelectric fields and growth. U. Texas Press, Austin.

[26] Mano, N. and Heller, A. (2005) Bioelectrochemical propulsion. *J. Am. Chem. Soc.* **127**(33):11574 – 11575.
doi: 10.1021/ja053937e.

[27] Mitchell, P. (1956) Hypothetical thermokinetic and electrokinetic mechanisms of locomotion in micro-organisms. *Proc. R. Phys. Soc. Edinburgh* **25**:32 – 34.

[28] Mitchell, P. (1972) Self-Electrophoretic locomotion in microorganisms – bacterial flagella as giant ionophores. *FEBS Letters* **28**(1):1 – 4.
doi: 10.1016/0014-5793(72)80661-6.

[29] Moran, J.L., Wheat, P.M. and Posner, J.D: (2010) Locomotion of electrocatalytic nanomotors due to reaction induced charge Auto-Electrophoresis. *Phys. Rev. E* **81**(6):065302.
doi: 10.1103/PhysRevE.81.065302.

[30] Moran, J.L. and Posner, J.D. Electrokinetic locomotion due to reaction induced charge electrophoresis. submitted to *J. Fluid Mech*. September 2010.

[31] Nuccitelli, R.and Jaffe, L.F. (1976) Ionic components of current pulses generated by developing fucoid eggs. *Dev. Biol.* **49**(2):518 – 531.
doi: 10.1016/0012-1606(76)90193-7.

[32] Paxton, W.F., Kistler, K.C., Olmeda, C.C., Sen, A., St Angelo, S.K., Cao, Y.Y., Mallouk, T.E., Lammert, P.E. and Crespi, V.H. (2004) Catalytic nanomotors: Autonomous movement of striped nanorods. *J. Am. Chem. Soc.* **126**(41):13424 – 13431. doi: 10.1021/ja047697z.

[33] Paxton, W.F., Sen, A. and Mallouk, T.E. (2005) Motility of catalytic nanoparticles through self-generated forces. *Chem.–Eur. J.* **11**(22):6462 – 6470. doi: 10.1002/chem.200500167.

[34] Paxton, W.F., Baker, P.T., Kline, T.R., Wang, Y., Mallouk, T.E. and Sen, A. (2006) Catalytically induced electrokinetics for motors and micropumps. *J. Am. Chem. Soc.* **128**(46):14881 – 14888. doi: 10.1021/ja0643164.

[35] Pitta, T.P. and Berg, H.C. (1995) Self-Electrophoresis is not the mechanism for motility in swimming cyanobacteria. *J. Bacteriol.* **177**(19):5701 – 5703.

[36] Purcell, E.M. (1977) Life at low reynolds number. *Am. J. Phys.* **45**(1):3 – 11. doi: 10.1119/1.10903.

[37] Sundararajan, S., Lammert, P.E., Zudans, A.W., Crespi, V.H. and Sen, A. (2008) Catalytic motors for transport of colloidal cargo. *Nano Letters* **8**(5):1271 – 1276. doi: 10.1021/nl072275j.

[38] Wang, Y., Hernandez, R.M., Bartlett, J., Bingham, J.M., Kline, T.R., Sen, A. and Mallouk, T.E. (2006) Bipolar electrochemical mechanism for the propulsion of catalytic nanomotors in hydrogen peroxide solutions. *Langmuir* **22**(25):10451 – 10456. doi: 10.1021/la0615950.

[39] Waterbury, J.B., Willey, J.M., Franks, D.G., Valois, F.W. and Watson, S.W. (1985) A cyanobacterium capable of swimming motility. *Science* **230**(4721):74 – 76. doi: 10.1126/science.230.4721.74.

[40] Yates, G.T. (1986) How microorganisms move through water. *Am. Sci.* **74**(4):358 – 365.

[41] Peter D. Mitchell was a British biochemist who was later awarded the 1978 Nobel Prize in Chemistry for his chemiosmotic mechanism of ATP synthesis.